*Progress In Electromagnetics Research C, Vol. 90, 265–279, 2019*

# DC Transformer Compensation for Efficiency Improvement of Electric Vehicles Wireless Charging Systems

**Yao He[1], Mei Liu[1, *], Xintian Liu[1], Xinxin Zheng[1], Guojian Zeng[1], and Jangfeng Zhang[2]**

**Abstract**—A wireless charging system for electric vehicles has two parts which are located inside and outside the vehicle respectively, and energy is transmitted from the outside part to inside part through a loosely coupled transformer. The energy transmission efficiency is directly related to the power conversion efficiency of the entire wireless charging system. This paper aims to improve the transmission efficiency of the DC transformer of the wireless charging system through studying compensation design method of DC transformer. A dual-tap rectifier is applied at the secondary side of the transformer, and a capacitor is connected in series on the primary side. Two capacitors are connected in series on the secondary side. By quantitative analysis on DC transformer efficiency, the relationship among efficiency, switching frequency, and compensation parameter is obtained. The compensated DC transformer realizes soft switch and further improves transformer efficiency. Finally, simulation and experiment on the wireless charging system with magnetic induction are conducted to verify the improved transformer design. The simulated and experimental results show that the average compensated DC transformer efficiency has been improved by 1.248%. Thus the designed DC transformer can effectively improve the energy transmission efficiency, and reduce voltage stress of the power device.

## 1. INTRODUCTION

Nowadays, the industry of electric vehicle (EV) is developing rapidly. Affected by key factors such as high cost and limited driving distance, EV has not been effectively promoted [1]. Charging technology is one of the key technologies of electric vehicle systems, which is of great significance to solve the limited driving distance challenge [2–6]. EV charging based on inductive wireless power transfer (IWPT) technology has evolved into a new era, and it is considered as robust, efficient (about 85–92%), and also reliable in harsh environments [7]. A wireless charging system does not use electric cables to charge the electric vehicle, and its contactless feature implies less wear, safer, and more convenient to use in a humid environment. Therefore, it is likely to become an important option for vehicle charging in the future to extend its driving distance [8–10].

In the wireless charging system, there is a large air gap between the primary and secondary sides of the DC transformer, resulting in a low coupling coefficient and a large leakage inductance, which not only affects the efficiency of wireless charging, but also increases the voltage stress and current stress of the power device [11, 12]. Therefore, it is necessary to optimize the DC transformer to improve the efficiency of wireless charging system. The methods to improve DC transformer transmission efficiency mainly include compensation, switch control, and core optimization. In [13], four capacitor compensation topologies of the primary-secondary side of DC transformer are investigated, which provides only the relevant compensation capacitance without simulation or experiment verification. In [14], a new burst mode control with constant burst-on time and optimal three-pulse switching mode is proposed to achieve

*Received 7 November 2018, Accepted 10 February 2019, Scheduled 6 March 2019*

* Corresponding author: Mei Liu (Liumei257248@163.com).

[1] Automobile Engineering Technology Research Institute, Hefei University of Technology, Hefei 230009, China. [2] School of Electrical and Data Engineering, University of Technology Sydney, NSW 2007, Australia.

high efficiency and minimum output voltage ripples, and this burst switch control may cause noise and affect battery life. In [15], a new pulse width modulation (PWM) control strategy is proposed to realize the optimal design of the magnetic components, which can reduce the switching loss and magnetic components loss to improve efficiency. However, the maximum voltage gain of the transformer is reduced, and this control strategy is not suitable for EV wireless charging system. In [16], a compensated transformer equivalent model is used to analyze the characteristics of the wireless charging system, but the working efficiency of the system is not maximized, and the output voltage varies with the load. Reference [17] designs only the compensation parameters in the four compensation models and does not discuss the effect of compensation parameters on efficiency. In order to solve these problems on wireless charging efficiency, this paper studies the compensation methods of loosely coupled DC transformer and relevant experimental verifications.

To be more specific, this paper will focus on the parameter design of capacitances and inductances for the compensation of loosely coupled DC transformer to improve energy transmission efficiency in electric vehicle wireless charging systems. A dual-tap rectifier is applied at the secondary side of the transformer, which reduces half of the diode losses compared to bridge rectification. After adding the compensation capacitor to the primary side and secondary side of the transformer, the peaks of voltage and current in the circuit are reduced, which can not only extend the life of the switch but also reduce EMI. This compensation does not require additional control switches and control signals, and the methodology is simple and very suitable for electric vehicle wireless charging. Moreover, for any given expected output power, the primary apparent power is an important parameter to measure energy transmission efficiency. Compensation technique can reduce unnecessary primary apparent power input and improve the transmission efficiency of the transformer. Simulated and experimental results demonstrate the correctness of the relevant theoretical analysis and the compensation design, and the output efficiency is increased by 1.248% on average compared to the double LCL compensation wireless charging technology.

The layout of the remaining sections is as follows. Section 2 studies the relationship between power transmission and coupling coefficients, compensation and efficiency, and compensation parameter design. It provides the guiding principles for compensation design to improve charging efficiency. In Section 3, simulations are performed, and an experimental prototype of the wireless charging system is built, which verifies that the theoretical design. Numerical simulation and experimental results are consistent. Finally, concluding remarks are provided in Section 4.

## 2. TRANSFORMER OUTPUT CHARACTERISTICS AND COMPENSATION ANALYSIS

### 2.1. Relationship between Apparent Power and Coupling Coefficient

Figure 1(a) shows the T-type equivalent circuit of DC transformer without compensation. $\dot{U}_{in}$ is the input voltage phasor, $U_{in}$ the input voltage rms value, $M$ the mutual inductance between the transmitter and the receiver, $L_P$ the primary winding inductance, $L_S$ the secondary winding inductance, $L_P - M$ the primary leakage inductance, and $L_S - M$ the secondary leakage inductance. Notation $\dot{I}_1$ is the primary input current phasor, $I_1$ the input current rms value, $\dot{I}_2$ the secondary current phasor, $I_2$ the secondary current rms value, $\omega$ the switching angular frequency, $R_L$ the load impedance, and $\dot{U}_0$ the output voltage phasor. Fig. 1(b) is T-type equivalent of primary compensated DC transformer, $C_1$ is the primary compensation capacitor. Fig. 1(c) is T-type equivalent of primary and secondary compensated DC transformer, $C_2$ is the secondary compensation capacitor. For the ease to analyze the circuit model of DC transformer, turns ratio $n$ is assumed to be one, and then

$$\dot{U}_{in} - j\omega L_p \dot{I}_1 - j\omega M \dot{I}_2 = 0 \tag{1}$$

$$\dot{I}_2(j\omega L_S + R_L) + j\omega M \dot{I}_1 = 0 \tag{2}$$

Assuming that the output power of the secondary side is $P_0$, from Eqs. (1) and (2) we can obtain

$$U_{in} = I_2 \sqrt{\left(\frac{L_P R_L}{M}\right)^2 + \omega^2 \left(\frac{L_P L_S}{M} - M\right)^2} \tag{3}$$

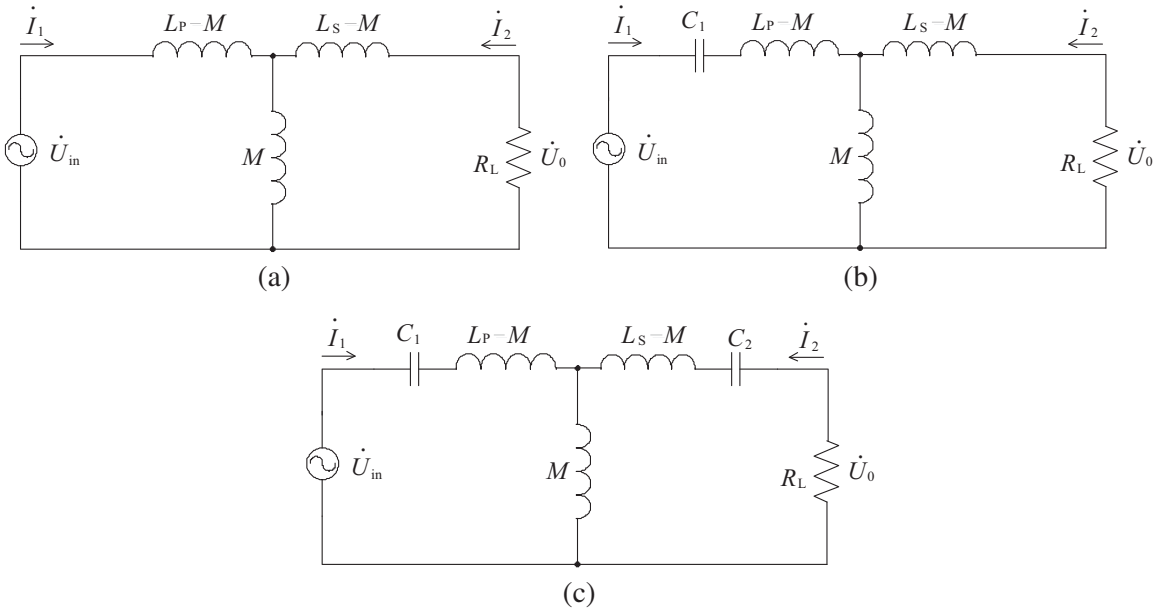


**Figure 1.** T-type equivalent circuit model of DC transformer with turns ratio. (a) Uncompensated DC transformer. (b) Primary compensated DC transformer. (c) Primary and secondary compensated DC transformer.

$$I_1 = I_2\sqrt{\frac{R_L^2+\omega^2L_S^2}{\omega^2M^2}} \tag{4}$$

According to the apparent power $S_P{=}U_{in}I_1$ and $P_0 = I_2^2R_L$, the primary side apparent power is calculated as follows:

$$S_P{=}\frac{P_0}{M^2R_2}\sqrt{\left(\frac{L_P^2R_L^4}{\omega^2}+\omega^2L_S^2\left(L_PL_S{-}M^2\right)^2+\left(L_PL_S{-}M^2\right)^2R_L^2+L_P^2L_S^2R_L^2\right)} \tag{5}$$

When $\frac{dS_P}{d\omega} = 0$

$$\omega_{\min}{=}R_L\sqrt{\frac{L_P}{L_S\left(L_PL_S{-}M^2\right)}} \tag{6}$$

$\omega_{\min}$ is the switching angular frequency when the apparent power of the transformer is minimum.

Let $k$ be the coupling coefficient of the loosely coupled transformer in the electric vehicle wireless charging system, and the uncompensated $k$ value is very low, usually equal to 0.2 [18]. The following relationship also holds:

$$k = \frac{M}{\sqrt{L_PL_S}} \tag{7}$$

From Eqs. (6) and (7) we can obtain

$$\omega_{\min} = \frac{R_L}{L_S\sqrt{1-k^2}} \tag{8}$$

From Eqs. (5) and (8) we have

$$\frac{S_{\min}}{P_0} = \frac{2-k^2}{k^2} \tag{9}$$

The minimum apparent power is $S_{\min}$ when $\omega{=}\omega_{\min}$. If the output power is constant, the minimum apparent power is related to the coupling coefficient. Fig. 2 shows the relationship of $S_{\min}/P_O$ and $k$, it can be seen that when the coupling coefficient is less than 0.2, the minimum apparent power and output

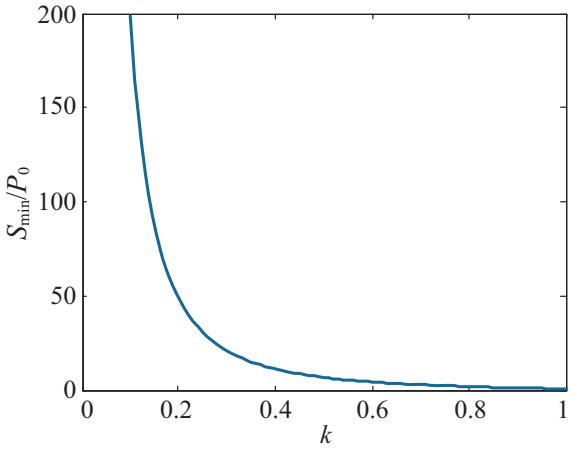


**Figure 2.** The relation between $S_{\min}/P_O$ and $k$.

power ratio is greater than 60. When the output power is constant, the minimum apparent power is much greater than the output power. Excessive apparent power increases the reactive power output, reduces the transmission efficiency of transformer, and increases the primary voltage stress [19].

### 2.2. The Effect of Compensation on Efficiency

Let $Z_{22}$ be the secondary impedance in Fig. 1(b), $Z_r$ the referred equivalent impedance of $Z_{22}$ to the transformer primary side [20], then

$$Z_r = \frac{(\omega M)^2}{Z_{22}} \tag{10}$$

$$Z_r = \frac{\omega^2 M^2}{\omega^2 L_S^2 + R_L^2} R_L - j\frac{\omega^3 M^3 L_S}{\omega^2 + L_S^2 + R_L^2} \tag{11}$$

The corresponding output power of the secondary side is:

$$P_0 = I_1^2 \mathrm{Re}(Zr) = \frac{I_1^2 \omega^2 M^2}{\omega^2 L_S^2 + R_L^2} R_L \tag{12}$$

From Eq. (12), we can see that $L_s$ limits its transmitted power. When $L_s$ is bigger, its transmitted power is smaller, which can make $P_0$ increase.

Figure 1(c) is the T-type equivalent circuit model of DC transformer with $n = 1$ and compensation from both the primary and secondary sides. The referred equivalent impedance of the secondary side impedance to the primary side can be calculated as:

$$Z_r = \frac{\omega^4 C_2^2 M^2 R_L}{\left(1 - \omega^2 C_2 L_S\right)^2 + \omega^2 C_2^2 R_L^2} + j\frac{\omega^3 C_2 M^2 \left(1 - \omega^2 C_2 L_S\right)}{\left(1 - \omega^2 C_2 L_S\right)^2 + \omega^2 C_2^2 R_L^2} \tag{13}$$

Assuming $\mathrm{Im}[Z_r] = 0$, $\omega_0$ is the resonant frequency, then the output power is:

$$P_O = I_1^2 \mathrm{Re}\left(Z_r\right) = \frac{I_1^2 \omega_O^2 M^2}{R_L} \tag{14}$$

According to Eq. (14), it can be seen that $L_s$ has no effect on the output power, and the load power is improved.

### 2.3. DC Transformer Compensation Circuit Topology

Through the analysis of the previous subsection, we can add the compensation capacitors $C_1$, $C_2$, $C_3$ at the primary side and the secondary side to improve the transmission efficiency of the wireless charging system. Fig. 3(a) illustrates the compensated DC transformer circuit.

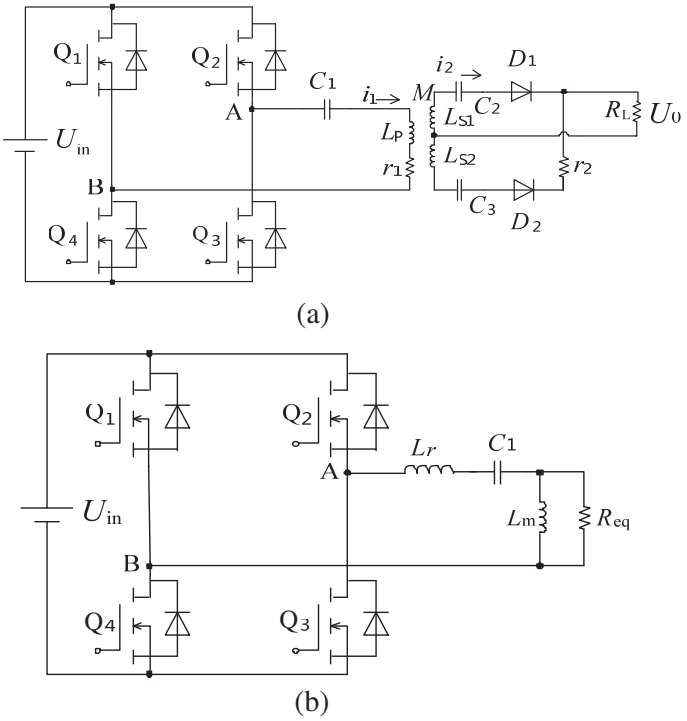


**Figure 3.** The compensation of DC transformer circuit. (a) Topology. (b) Equivalent circuit of LLC.

After the addition of capacitors $C_1$, $C_2$, $C_3$, the AC voltage flows through the compensated DC transformer circuit, resulting in high-frequency resonance, and the resonant voltage is rectified and passed to electric vehicles. The DC transformer leakage inductance and excitation inductance and capacitance are equivalent to those in the LLC-DC transformer.

In the design of DC transformer, it needs to reduce the leakage inductance between the primary and secondary windings [21], while in the design of LLC resonant converter, the leakage inductance between the primary and secondary can be used as resonant inductance [22]. Therefore, in the design of LLC-DC transformer, the values of the leakage inductance should be taken into account. Fig. 3(b) is an equivalent circuit of Fig. 3(a) when the secondary side impedance is referred to the primary side.

In Fig. 3(b), $C_1$ is the resonant capacitor, $L_m$ the excitation inductance, and $L_r$ the transformer leakage inductance. The elements $C_1$, $L_m$ and $L_r$ constitute the LLC resonant circuit, where $C_1$ can block DC current and can also balance the magnetic field of transformer in order to prevent the magnetic saturation of DC transformer. Ignoring the leakage inductance at the transformer secondary side, the rectifier circuit and the load are equivalent to a resistance $R_{eq}$ in Fig. 3(b) [23]:

$$R_{eq} = \frac{8}{\pi^2} * n^2 * R_L \tag{15}$$

where $R_L$ is the load, and $n$ is the primary-to-secondary DC transformer turns ratio.

The input-output transfer function $G(j\omega)$ is as follows:

$$G\left(j\omega\right) = \frac{-\omega^2 L_r C_1}{-\omega^2 L_r C_1 - \omega^2 L_r C_1 \left(jQ\omega\sqrt{L_r C_1} + \dfrac{L_r}{L_m}\right) + jQ\omega\sqrt{L_r C_1} + \frac{L_r}{L_m}} \tag{16}$$

where $Q = \frac{1}{R_{eq}}\sqrt{\frac{L_r}{C_1}}$, $\omega_0 = \frac{1}{\sqrt{L_r C_1}}$, $\frac{\omega}{\omega_0} = \frac{f}{f_0}$, $f$ is the switching frequency, and $f_0$ is the resonant frequency which can be determined by $L_r$ and $C_1$.

Assuming that $K = L_r/L_m$ and $f_n = f/f_0$, $G(j\omega)$ can be simplified as

$$G(j\omega) = \frac{1}{1 + K - \frac{K}{f_n^2} + jQ\left(f_n - \frac{1}{f_n}\right)} \tag{17}$$

Input and output voltage gain can be calculated by:

$$M = \frac{\frac{1}{2n}}{\sqrt{\left(1 + K - \frac{K}{f_n^2}\right)^2 + Q^2\left(f_n - \frac{1}{f_n}\right)^2}} \tag{18}$$

The DC transformer parameters are set such that the turns ratio $n = 1$, $Q = 1$. It can be seen from Fig. 4 that the voltage gain $M$ is high when the ratio $f_n$ approaches 1, and the value of $K = L_r/L_m$ is kept unchanged. When $f_n$ and excitation inductance $L_m$ are constant, the voltage gain $M$ turns bigger with the increase of the leakage inductance $L_r$. When the leakage inductance $L_r$ reaches a certain value, the voltage gain reaches maximum. When the leakage inductance $L_r$ is further increased, the voltage gain will drop. In other words, in the design of DC transformer, the leakage inductance cannot be infinitely increased.

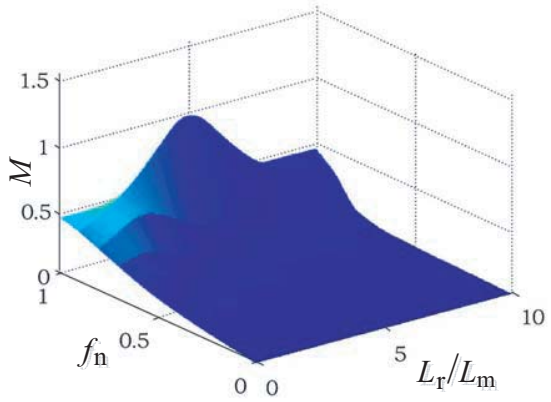


**Figure 4.** Relationship of DC transformer output, leakage inductance and frequency ratio.

## 3. SYSTEM DESIGN AND EXPERIMENTAL VERIFICATION

### 3.1. System Design and Simulation Analysis

The optimized angular frequency $\omega_{opt}$ is the angular frequency of the input power when the apparent power of the system is minimal. Denote the ratio of the resonant angular frequency to the optimized angular frequency by $p = \omega_0/\omega_{opt}$. When the resonant angular frequency deviates from the optimum angular frequency, notation $y$ can be defined to characterize the rate of increase of the apparent power: $y = (S_p - S_{\min})/S_{\min}$.

Figure 5 shows the apparent power increase rate with the coupling coefficient $k$ and $p$ changes the surface. It can be seen that when resonant angular frequency is not equal to the optimum angular frequency, the apparent power will increase.

Relations among $S_P/P_O$, $R$, and $\omega$ are shown in Fig. 6, and it can be found that when the DC transformer is compensated, the ratio of apparent power and output power decreases for fixed $R$ and increasing $\omega$. Compared with uncompensated DC transformer, the primary side after capacitor compensation can reduce its apparent power and improve DC transformer power factor.

Based on the previous analysis, DC transformer needs to work in the optimal frequency $\omega_0$ in order to reduce the apparent power of DC transformer and achieve maximum load active power. Formula (19)

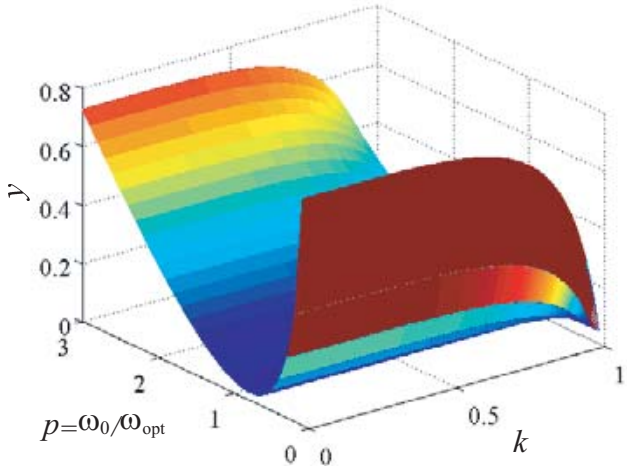


**Figure 5.** Plot of $y$ as a function of $k$ and $p$.

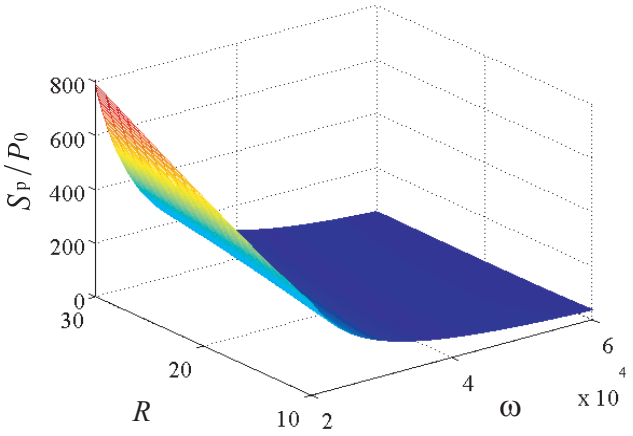


**Figure 6.** Plot of $S_P/P_O$ as a function of $R$ and $\omega$.

is the impedance of the secondary side when the secondary side is compensated. Assuming that the secondary inductance and operating frequency are given, the secondary compensation capacitor $C_2$ can be determined as Equation (20):

$$Z_{22} = j\omega L_{s1} + \frac{1}{j\omega C_2} + R_L \tag{19}$$

$$C_2 = \frac{1}{\omega_o^2 L_{S1}} \tag{20}$$

Since the design of the loosely coupled transformer is the double tap output, $C_3$ is equal to $C_2$. Equation (14) shows that the referred equivalent impedance of the series compensated secondary side impedance to the primary side will be purely resistive. The resulting primary side equivalent impedance $Z_{SS}$ is as follows:

$$Z_{SS} = \frac{\omega_o^2 M^2}{R_L} + j\omega_o L_p + \frac{1}{j\omega_o C_1} \tag{21}$$

In order to maximize the primary input current, the imaginary part of $Z_{SS}$ needs to be zero. Therefore, the primary compensation capacitor $C_1$ is:

$$C_1 = \frac{1}{\omega_o^2 L_p} \tag{22}$$

The circuit simulation model is established in MATLAB. Table 1 shows the simulation parameters.

**Table 1.** Simulation parameters.

| | |
|---|---|
| $U_{in}$ | 400 V |
| $L_P$ | 230 µH |
| $L_{S2}$ | 215 µH |
| $C_2$ | 47 nF |
| $f_0$ | 100 kHZ |
| $L_{S1}$ | 215 µH |
| $C_1$ | 47 nF |
| $C_3$ | 47 nF |

With the simulation parameters in Table 1, Fig. 7 shows the simulation voltage and current results of the DC transformer. As the switch and transformer are connected in series, the switch current is equal to the transformer current, and the turn-off voltage of the switch is equal to the transformer voltage. It can be seen from Fig. 7(a) that the voltage spikes are big, and the current is small when DC transformer is uncompensated. The voltage spikes will produce a large switching stress on the device [11] and will produce electromagnetic interference and noise. Small excitation current will reduce the transmission efficiency of the transformer. Fig. 7(b) shows that the voltage spike of the primary side compensated DC transformer tends to be gentle, and the voltage stress is reduced compared to the uncompensated case in Fig. 7(a); however, the current oscillation is large. Fig. 7(c) gives the results of compensation

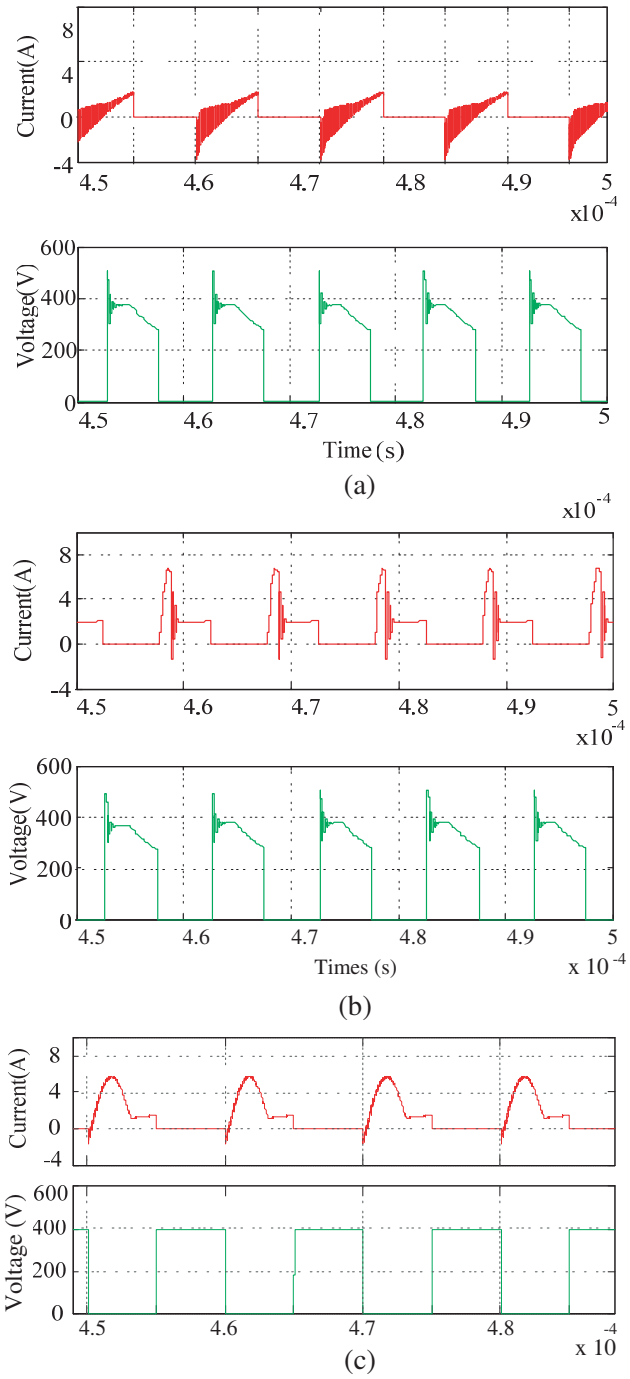

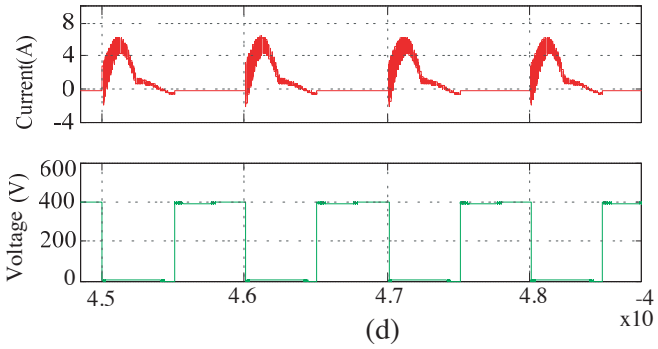


**Figure 7.** Switch current and voltage. (a) Uncompensated DC transformer. (b) Primary side compensated DC transformer. (c) Primary and secondary compensated DC transformer (Including C1, C2 and C3). (d) Primary and secondary compensated DC transformer ($C1 = 0.5C2 = 0.5C3$).

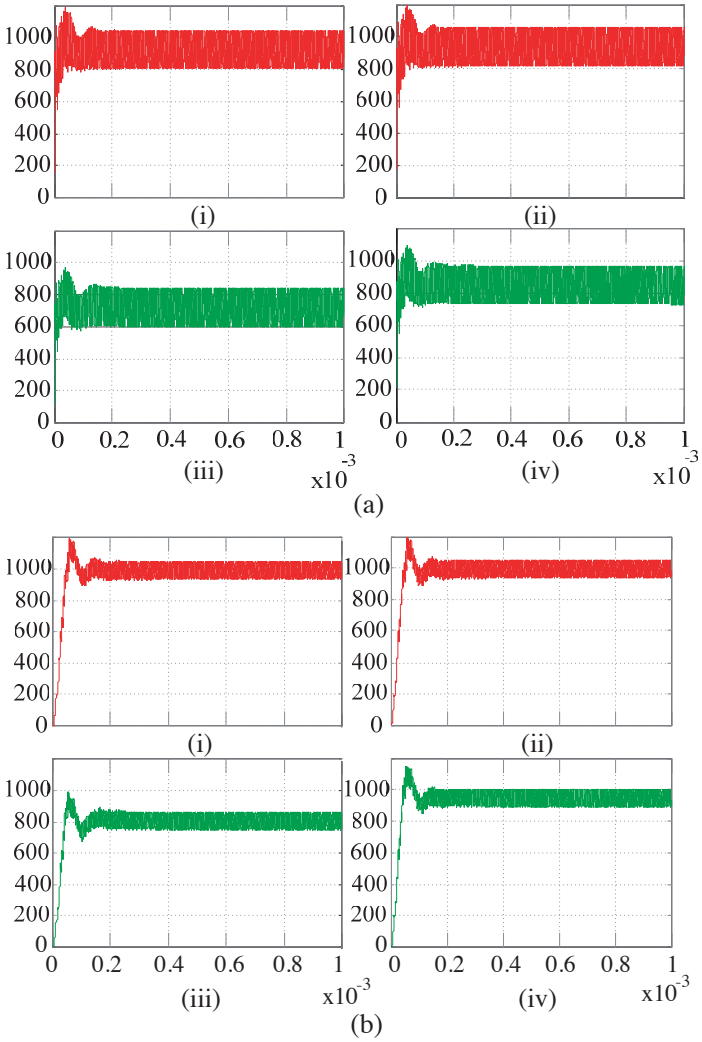


**Figure 8.** Input and output power of the DC transformer at different loads. (a) Uncompensated DC transformer. (b) Primary and secondary compensated DC transformer.

from both primary and secondary sides, which shows that both the current spike of DC transformer and the current stress of the switch are reduced compared to Fig. 7(a). The voltage spikes phenomenon and device switching losses are reduced accordingly. The parasitic parameters in the compensation capacitor absorption circuit are used at switching resonance devices and eliminate the voltage spike and inrush current caused by the parasitic parameter at high frequency, thus greatly reduces the switching stress of the device. Fig. 7(d) is the circuit in the non-resonant conditions of the simulation, where the imaginary value of the impedance $Z_{SS}$ is not equal to zero. Since the imaginary value of the impedance is not equal to zero, transformer input current is smaller than that of Fig. 7(c), and transmission efficiency is also smaller than Fig. 7(c).

Figures 8(a) and (b) are the input (subfigures (i) and (ii)) and output (subfigures (iii) and (iv)) active power simulation of the DC transformer, in which (i) and (iii) are simulated at 50% of rated load, and (ii) and (iv) are at the full load. From (iii) and (iv) we can see that the output power increases at full load, so the transmission efficiency of the transformer is related to the load. Comparing Figs. 8(a) and (b), it can be concluded that the DC transformer transmission efficiency after compensation is increased under both load conditions, and the oscillation is also reduced.

### 3.2. Experimental Results and Discussion

Figure 9 is a wireless charging DC transformer experiment platform with the switching frequency 50 kHz and out power 1 kW, which is designed to verify the results in this paper. The input voltage is 400 V, and the output voltage is 398.5 V. DC transformer core material is ferrite EE42, and transformer turns ratio $n_1 : n_2$ is 1 : 1. The primary side has 4 shares 0.5 mm Leeds line parallel and is wound 25 turns. DC transformer secondary side has also 4 shares 0.5 mm Leeds line in parallel, and the turns are the same as the primary side.

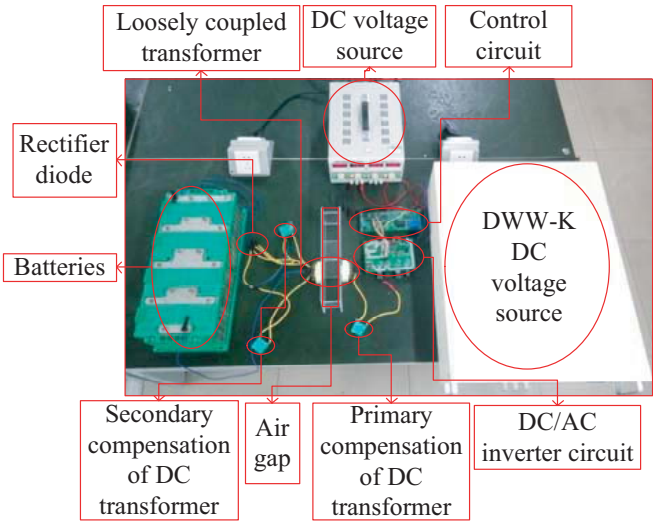


**Figure 9.** The experiment platform of the wireless charging DC transformer.

Figure 10(a) gives the drain-source voltage $u_{ds}$ and the current $i_s$ of the uncompensated DC transformer. It can be seen that when the loosely coupled DC transformer is not compensated, there are voltage spikes and oscillation at both ends of the switch. The current is very small, and oscillations are large, which increases the stress of the switch. The transmission efficiency of the transformer is low. Fig. 10(b) shows the primary side compensated DC transformer waveform. Compared with Fig. 10(a), it is found that the compensated DC transformer current increases and that the transformer efficiency increases, but the voltage spikes are not completely disappear. When the switch is turned off, $u_{ds}$ is gradually increasing, but $i_s$ is not zero, thus the circuit is not soft-switching and still consumes certain power. When both the primary and secondary sides are compensated as shown in Fig. 10(c), the voltage and current waveform spikes are reduced further so that voltage stress and current stress of the switch

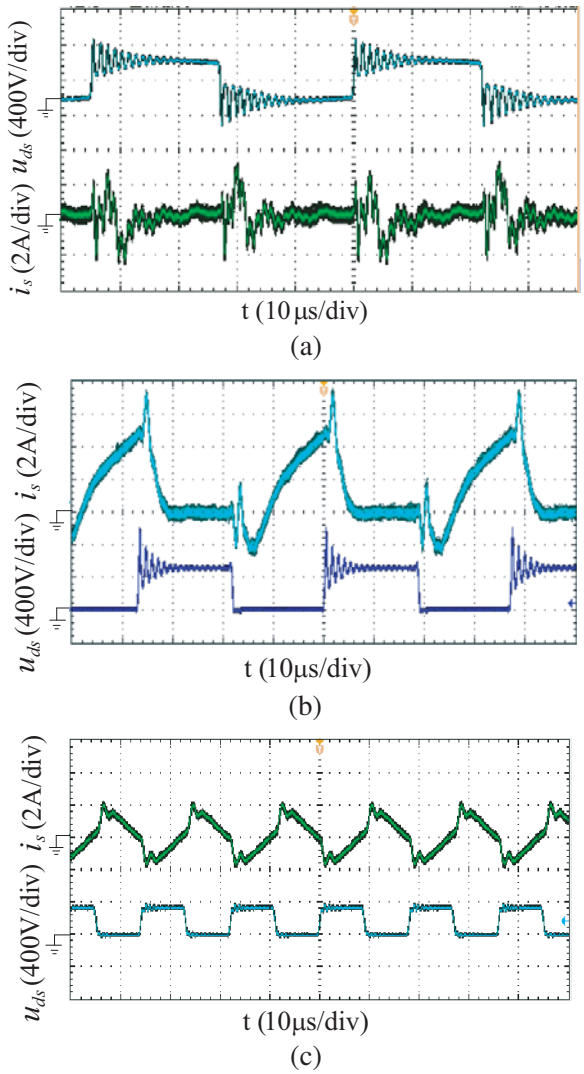


**Figure 10.** Switch current and voltage experimental waveforms. (a) Uncompensated. (b) Compensated primary side. (c) Compensated primary and secondary sides.

are further relieved compared with Fig. 10(b). The current is significantly increased, so the efficiency is improved. When the switch is closed, $u_{ds}$ drops to zero, and $i_s$ gradually increases from zero which achieves the zero-voltage turn-on; when the switch is open, $i_s$ is reduced to zero, and $u_{ds}$ is gradually increasing to achieve zero-current turn-off, thus DC transformer achieves soft-switching, and the reverse recovery loss of the switch is reduced.

Figure 11 shows the output voltage waveforms of the two-side compensated DC transformer under different distances between the primary and secondary sides of the transformer. It can been seen that as the distance between the primary side and secondary side increases from zero, the voltage spike of the DC transformer is reduced, but stable voltage values remain the same, and the leakage inductance of the transformer also gradually increases. However, when the distance between the primary and secondary side is greater than 40 mm, the output voltage drops sharply. Therefore, the leakage inductance of DC transformer can be used as the resonant inductor to reduce the output voltage spike and reduce the voltage stress.

Table 2 is the output efficiency of secondary-side double-tap loosely coupled transformer at different loads under different compensation scenarios: uncompensated, primary side compensated, and both primary and secondary compensated. Fig. 12 plots the relevant efficiency curve for the comparison

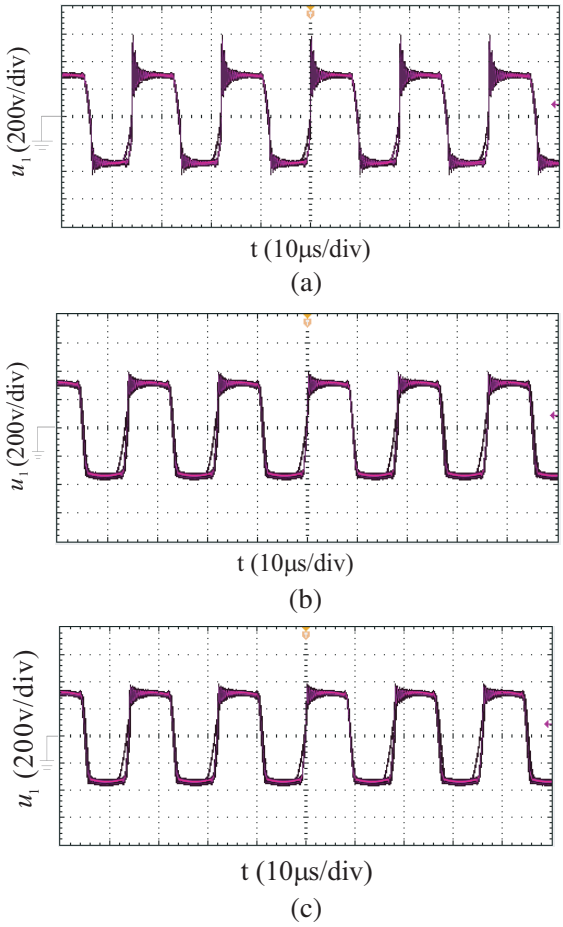


**Figure 11.** Output voltage waveform of DC transformer with compensated primary and the secondary sides at different distances. (a) $h = 0$ mm. (b) $h = 20$ mm. (c) $h = 40$ mm.

**Table 2.** Transmission efficiency of DC transformer at different load.

| Load percent (%) | 25 | 50 | 75 | 100 |
|---|---|---|---|---|
| Uncompensated (%) | 71.82 | 80.77 | 86.62 | 86.89 |
| Primary compensated (%) | 75.53 | 83.56 | 90.54 | 89.99 |
| Primary and secondary Compensated (%) | 76.95 | 85.88 | 91.73 | 90.51 |

of the three scenarios. It is observed that the output efficiency increases with the increase of the load, and the output efficiency reaches a maximum value when the load percentage reaches 80% in all three compensation scenarios. The DC transformer average output efficiency of the primary-secondary compensated wireless charging is 4.549% higher than that of the uncompensated case. The efficiency of the primary compensation is between the uncompensated scenario and both primary and secondary compensated scenarios. The output efficiency can go up to 93.82% when both primary and secondary scenarios are compensated. This comparison shows that transmission efficiency has been effectively improved by the newly designed primary-secondary compensated DC transformer. Table 3 shows the compensation parameters for this paper and other recent studies, and the transmission efficiency is measured under the same load conditions. The compensation method S-S chosen in this paper can reduce the parameter matching and reduce the volume and cost compared with the double LCL compensation method [15], and indeed, the DC transformer average transformer efficiency can be improved by 1.248%

**Table 3.** The parameters of the compensation method.

| Compensation method | Primary side | Secondary side | Transmission efficiency |
|---|---|---|---|
| S-S | $C_1$ | $C_2$, $C_3$ (double-tap) | 93.826% |
| Double LCL | $L_P$, $C_1$ | $L_S$, $C_2$ | 92.578% |
| LLC | $C_1$ | No capacitance and inductance | 90.274% |

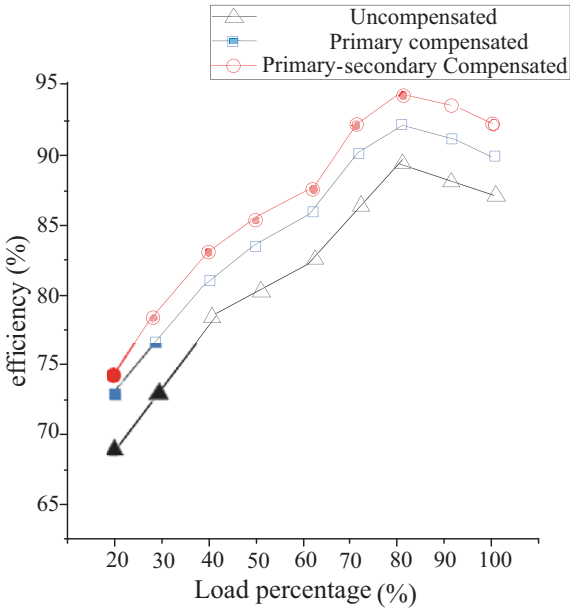


**Figure 12.** The efficiency curve of the DC transformer.

compared to [15]. Compared with the LLC technology in [4], the secondary series compensation capacitor can reduce the effect of load variation on the optimized frequency, and our new method can improve efficiency by 2.552%.

## 4. CONCLUSIONS

In this paper, the compensation method of the loosely coupled DC transformer with open loop control at primary side and double-tap uncontrolled rectification at secondary side is introduced. The effects of compensation capacitors $C_1$, $C_2$, and $C_3$ on the output efficiency of the transformer and the apparent power of the primary side are analyzed. Finally, the charging experiment platform is established. The simulated and experimental results show that after the compensation capacitors are added to the transformer primary and secondary sides, and the input apparent power and primary power capacity requirements are reduced. Transformer can achieve soft-switching, and the voltage and current stresses of the switch and the energy losses are also reduced. The leakage inductance is considered in the compensation circuit, which makes it more suitable for practical application. When the transformer load is 80% of rated load, the transformer reaches the maximum transmission efficiency of 93.82%. Compared with the double LCL compensation method and LLC compensation method, the newly proposed compensation method can improve efficiency by 1.248% and 2.552%, respectively. From practical point of view, this method does not need additional control parts and has fewer matching parameters. It not only reduces the cost, but also improves the efficiency of transformer. In addition, it reduces the impact of load changes on transformer efficiency. As a future work, we will apply compensation techniques to further optimize the core structure and coil winding method of the transformer to improve the efficiency of wireless charging.

## APPENDIX A.

| | |
|---|---|
| $\dot{\mathrm{U}}_{in}$ | Transformer input voltage phasor (V) |
| $U_{in}$ | Transformer input voltage rms value (V) |
| $U_0$ | Load voltage (V) |
| $M$ | Mutual inductance (μH) |
| $L_P$ | Primary winding inductance (μH) |
| $L_S$ | Secondary winding inductance (μH) |
| $\dot{\mathrm{I}}_1$ | Primary input current phasor (A) |
| $I_1$ | Primary input current rms value (A) |
| $\dot{\mathrm{I}}_2$ | Secondary current phasor (A) |
| $I_2$ | Secondary current rms value (A) |
| $\omega_0$ | Resonant angular frequency (rad/s) |
| $C_1$ | Primary compensation capacitor (nF) |
| $C_2$, $C_3$ | Secondary compensation capacitor (nF) |
| $R_L$ | Load impedance (Ω) |
| $k$ | Coupling coefficient |
| $S_P$ | Apparent power (MVA) |
| $S_{\min}$ | Minimum apparent power (MVA) |
| $P_0$ | Load power (kW) |
| $\omega_{opt}$ | Optimize the angular frequency (rad/s) |
| $Z_{22}$ | Secondary impedance (Ω) |
| $Z_r$ | Equivalent impedance (Ω) |
| $G$ | Voltage gain |
| $L_r$ | Transformer leakage inductance (μH) |
| $L_m$ | Excitation inductance (μH) |
| $f_0$ | Resonant frequency (kHz) |

## REFERENCES


1. Bhatti, A. R., "A comprehensive overview of electric vehicle charging using renewable energy," *International Journal of Power Electronics & Drive Systems*, Vol. 7, No. 1, 114–123, Mar. 2016.
2. Chuen, I. P. S., "Charging support in Battery Electric Vehicle (BEV) development," *2017 7th International Conference on Power Electronics Systems and Applications — Smart Mobility, Power Transfer & Security (PESA)*, 1–4, Hong Kong, 2017.
3. Zheng, Y., "Online distributed MPC-based optimal scheduling for EV charging stations in distribution systems," *IEEE Transactions on Industrial Informatics*, 1–1, 2018.
4. Zhang, W., "Decentralized electric vehicle charging strategies for reduced load variation and guaranteed charge completion in regional distribution grids," *Energies*, Vol. 10, No. 2, 147, Jan. 2017.
5. Liu, F., "Transmitter-side control of both the CC and CV modes for the wireless EV charging system with the weak communication," *IEEE Journal of Emerging & Selected Topics in Power Electronics*, Vol. 6, No. 2, 955–965, Oct. 2018.
6. Purwadi, A., "Analysis of power converters for high frequency resonant inductive electric vehicle charging system," *2016 3rd Conference on Power Engineering and Renewable Energy*, 159–164, 2017.

7. Hata, K., "Proposal of classification and design strategies for wireless power transfer based on specification of transmitter-side and receiver-side voltages and power requirements," *IEEJ Transactions on Industry Applications*, Vol. 138, No. 4, 330–339, Apr. 2018.
8. Fujita, T., "Fundamental discussion on a wireless power transfer system equipped with a common secondary coil during parking and driving," *IEEJ Transactions on Industry Applications*, Vol. 136, No. 8, 522–531, Aug. 2016.
9. Kan, T., "A new integration method for an electric vehicle wireless charging system using LCC compensation topology: Analysis and design," *IEEE Transactions on Power Electronics*, Vol. 32, No. 2, 1638–1650, Apr. 2017.
10. Imura, T., "Wireless power transfer for electric vehicle at the kilohertz band," *IEEJ Transactions on Electrical & Electronic Engineering*, Vol. 11, No. S2, S91–S99, Apr. 2016.
11. Knaisch, K., "Gaussian process surrogate model for the design of circular, planar coils used in inductive power transfer for electric vehicles," *IET Power Electronics*, Vol. 9, No. 15, 2786–2794, Dec. 2016.
12. Aworo, O. J., "Transformer for contactless electric vehicle charging with bidirectional power flow," *2017 IEEE Power & Energy Society General Meeting*, 1–5, 2017.
13. Bi, Z., "A review of wireless power transfer for electric vehicles: Prospects to enhance sustainable mobility," *Applied Energy*, Vol. 179, No. 1, 413–425, Oct. 2016.
14. Evzelman, M., "Burst mode control and switched-capacitor converters losses," *2016 IEEE Applied Power Electronics Conference and Exposition(APEC)*, 1603–1607, 2016.
15. Kim, J. W., "APWM adapted half-bridge LLC converter with voltage doubler rectifier for improving light load efficiency," *Electronics Letters*, Vol. 53, No. 5, 339–341, Mar. 2017.
16. Liu, C., "Double-LCL resonant compensation network for electric vehicles wireless power transfer: Experimental study and analysis," *IET Power Electron*, Vol. 9, No. 11, 2262–2270, Sep. 2016.
17. Li, W., "Inter-operability considerations of the double-sided LCC compensated wireless charger for electric vehicle and plug-in hybrid electric vehicle applications," *2015 IEEE PELS Workshop on Emerging Technologies: Wireless Power*, 1–6, 2015.
18. Kan, T., "A new integration method for an electric vehicle wireless charging system using LCC compensation topology: Analysis and design," *IEEE Transactions on Power Electronics*, Vol. 32, No. 2, 1638–1650, Feb. 2017.
19. Cai, H., "Output power adjustment in inductively coupled power transfer system," *Transactions of China Electrotechnical Society*, Vol. 29, No. 1, 215–220, Feb. 2014.
20. Huang, C. P. and D. B. Lin, "Signal integrity improvements of bended coupled lines by using miniaturized capacitance and inductance compensation structures," *2016 Asia-Pacific International Symposium on Electromagnetic Compatibility*, 22–24, 2016.
21. Gao, Y., "Safety and efficiency of the wireless charging of electric vehicles," *Proceedings of the Institution of Mechanical Engineers, Part D: Journal of Automobile Engineering*, Vol. 230, No. 9, 1196–1207, Sep. 2016.
22. Guan, Y., "A high-frequency CLCL converter based on leakage inductance and variable width winding planar magnetics," *IEEE Transactions on Industrial Electronics*, Vol. 65, No. 1, 280–290, Jan. 2018.
23. Zhang, W. and S. C. Wong, "Analysis and comparison of secondary series-and parallel-compensated inductive power transfer systems operating for optimal efficiency and load-independent voltage-transfer ratio," *IEEE Transactions on Power Electronics*, Vol. 29, No. 6, 2979–2990, Jun. 2014.